nzsee
NEW ZEALAND SOCIETY FOR EARTHQUAKE ENGINEERING

Experimental study on structural performance and damage characteristics of repaired flexural RC members

K. Miura, T. Anabuki & K. Yonezawa
Obayashi Corporation, Japan.

A. Mikawa, T. Nagai & M. Maeda
Tohoku University, Japan.

A.V. Shegay
Tokyo Institute of Technology, Japan.

M. Seki
Building Research Institute, Japan.

ABSTRACT

Understanding the expected seismic performance recovery of repaired members is important to make an effective recovery plan for damaged buildings. In this research, three RC beam and three RC wall specimens were subjected to pseudo-static loading to determine the seismic performance recovery following repair. Repair was undertaken using general methods such as epoxy injection and mortar patching. Two scenarios of damage level were considered prior to initiating repair: moderate and severe. Results of this study showed that spalling of concrete in repaired members was less than that observed in the original members. Initial stiffness recovery of 0.45 to 0.55 of the original members was achieved, regardless of the initial damage level. Secant stiffness at the yielding point of the repaired members recovered 0.85 to 0.95 in moderately damaged specimens while in severely damaged specimens, recovery was 0.75 to 0.9. Structural strength of the repaired members was found to be equivalent to that of the original members in moderately damaged cases and 1.1 to 1.2 of the original in severely damaged cases. Energy absorption capacity recovery was more than 0.8 in moderately damaged members and more than 0.4 in severely damaged members. Finally, crack characteristics were studied based on visual observations taken during the experiment. It was observed that more than half of cracks injected with epoxy resin reopened upon

loading, which explained the low recovery of initial stiffness. Crack width data showed that wider cracks are generally less likely to reopen following repair because of better epoxy penetration.

1 INTRODUCTION

Understanding the expected seismic performance recovery of repaired structural members is important to make an effective recovery plan for damaged buildings. Regarding expected structural performance recovery factor of reinforced concrete (RC) buildings, one existing document is Federal Emergency Management Agency's 'Evaluation of Earthquake Damaged Concrete and Masonry Wall Buildings' (FEMA 306 (1998)). In FEMA 306, the performance recovery factors for strength, secant stiffness to yield and deformation capacity are provided for RC walls and coupling beams. However, since the target building type is wall buildings, performance recovery factors for moment-frame components such as beams and columns are not included. In addition, recovery factors for energy absorption capacity are not considered. Another document for performance recovery factors of repaired RC members is Japan Building Disaster Prevention Association's 'Guidelines for Damage Classification Criteria and Restoration Techniques of Damaged Buildings' (JBDPA 2015). In this guideline, performance recovery factors for beams, columns and walls are provided corresponding to various damage levels and repair methods. However, these performance recovery factors are given as conservative values due to insufficient experimental data. Moreover, the recovery ratios are only defined for overall structural performance; thus, recovery factors for each performance characteristic (i.e., strength, stiffness, energy absorption) are unknown. Previous investigations on evaluating recovery factors for each performance characteristic was carried out by Shegay et al. (2023) via a shake-table test of 1/4 scale 4-story RC structure. However, since this research focused on the performance recovery factors of the frame as a whole, the recovery factors of each member type were unclear.

In this paper, three RC beam and three RC wall specimens were subjected to pseudo-static loading and their seismic performance recovery following repair were investigated. Furthermore, the effectiveness of repair was discussed through the results of observational survey of cracks.

2 EXPERIMENTAL PLAN

2.1 Test specimens

Three identical specimens were constructed each for RC wall and beam members. The first specimen of each member type was tested to failure, while the remaining two were subjected to a predetermined target damage state, repaired, and then retested to failure. RC wall and beam specimens were designed based on members in the longitudinal direction of the 1/4 scale 4-story structure tested in a previous study (Shegay et al. 2023). The wall specimens were 1/3 scale and corresponded to the wall in the 1st and 2nd stories (from the bottom to the contra-flexure point) of the 4-story structure. The beam specimens were half-scale and corresponded half the beam span length of the 4-story structure (from column face to the contra-flexure point). The list of the specimens is shown in Table 1 and the drawings of the specimens are shown in Figure 1. The term 'original' is given to the specimens tested from an undamaged state and 'repaired' is given to specimens tested after repair of damage. The numbers included in the names of the specimens indicate the target damage levels after first loading (loading before repair). Two target damage levels were considered: damage level II and IV. The adopted definitions of damage levels are taken from the JBDPA Guideline (2015), the summary of which is shown in Table 2. Material properties of concrete and steel reinforcement are shown in Table 3 and Table 4.

Table 1: List of specimens.

Member	Specimen		Target damage level	Note	Size (mm)	Reinforcement
Wall	Original	W2	II		100 × 900	Longitudinal bar: 24-D13 Hoop: D6@90
		W4	IV			
		W5	V			
	Repaired	W2R	V	W2 repaired		
		W4R	V	W4 repaired		
Beam	Original	G2	II		200 × 280	Longitudinal bar: 3+3-D13 Stirrup: D6@65
		G4	IV			
		G5	V			
	Repaired	G2R	V	G2 repaired		
		G4R	V	G4 repaired		

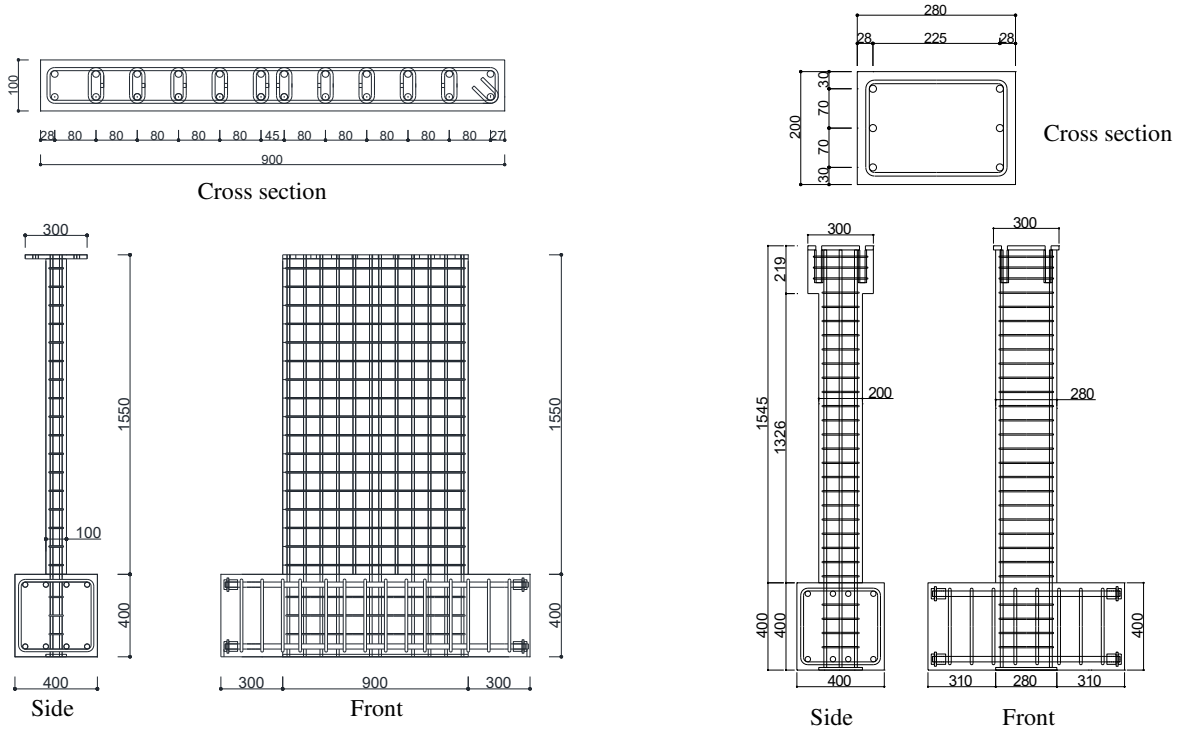

Figure 1: Drawings of specimens

Table 2: Definition of damage levels of structural members.

Damage level	Observed damage in structural members
I	Sparse cracks can be observed (<0.2 mm). No reinforcement yielding expected.
II	Clearly visible cracks (0.2 - 1 mm) exist. Reinforcement yielding expected.
III	Wide cracks (1 - 2 mm) are present. Plastic hinging mechanisms begin to form. Some spalling of cover concrete is observed but concrete core is in-tact.
IV	Many wide cracks are observed. Compression damage resulting in concrete spalling and exposed reinforcement. Lateral strength degradation may occur, but vertical load is still fully carried by walls and columns.
V	Buckling (and in some cases fracture) of reinforcement, crushing of concrete and vertical deformation of columns and/or shear walls observed. Settlement and inclination of structure are characteristic.

Table 3: Material properties of concrete.

Specimen	Nominal strength (N/mm^2)	Age (day)	Young's modulus (N/mm^2)	Compressive strength (N/mm^2)
W2	42	47	3.28×10^4	49.2
W4		38	3.41×10^4	47.8
W5		52	3.26×10^4	46.1
W2R		84	3.23×10^4	49.3
W4R		95	3.29×10^4	50.2
G2		75	3.28×10^4	48.6
G4		74	3.31×10^4	48.0
G5		63	3.27×10^4	49.3
G2R		171	3.34×10^4	52.7
G4R		181	3.27×10^4	53.2

Table 4: Material properties of steel reinforcement.

Diameter (Grade)	Young's modulus (N/mm^2)	Yield strength (N/mm^2)	Ultimate strength (N/mm^2)
D13(SD345)	1.87×10^5	380	562
D6(SD295)	1.76×10^5	364	546

2.2 Loading method

The test set up is shown in Figure 2. Two horizontal actuators (one in case of the beam specimen) were connected to the upper part of the specimen via a steel beam, and static cyclic loading was performed. The loading protocols of each specimen are shown in Figure 3. Two cycles were applied at each displacement level. Original specimens were loaded until they reached the target damage level shown in Table 1, while the repaired specimens were loaded until failure. In Figure 3, the relationships between the damage levels and the drift angle of the original specimens are shown.

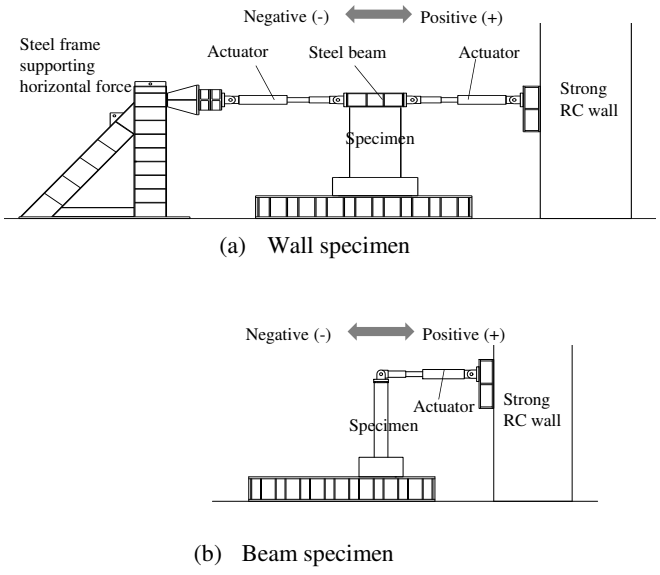

Figure 2: Test set up

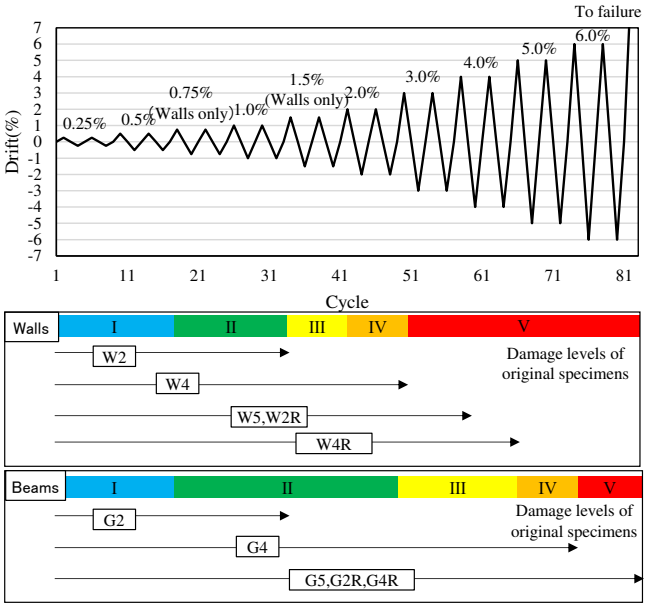

Figure 3: Loading protocols

2.3 Repair work

Following the loading of the original specimens, repair work was performed after the residual deformation was returned to almost zero. The concept of the repair work was to use general methods practiced in Japan. The specimens with damage level II (W2R, G2R) were repaired by epoxy injection of cracks. In the specimens with damage level IV (W4R, G4R), mortar patching was applied to areas where spalling of concrete was observed in addition to epoxy injection of cracks. Polymer cement mortar was used for minor spalling, and epoxy mortar was used for severe spalling where reinforcement was exposed. Material

properties of mortar are shown in Table 5, and repair process is shown in Figure 4. As a reference, the strength of the epoxy resin in the manufacturer's catalogue is also shown in Table 5.

Table 5: Material properties of mortar and epoxy resin.

Material	Specimen	Age (day)	Young's modulus (N/mm^2)	Compressive strength (N/mm^2)
Polymer cement mortar	W4R	33	2.71×10^4	55.5
	G4R	63	2.01×10^4	58.5
Epoxy mortar	W4R	33	1.88×10^4	90.5
	G4R	63	1.29×10^4	71.1
			Adhesive strength (N/mm^2)	Tensile strength (N/mm^2)
Epoxy resin	All		10.4	48.2

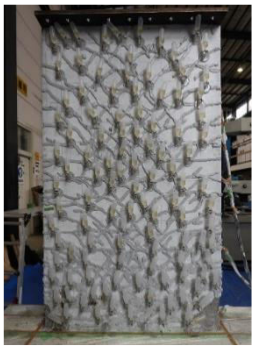

Epoxy injection

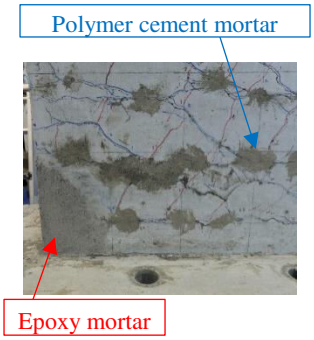

Mortar patching

3 TEST RESULTS

3.1 Damage process

The damage state of the wall specimens at drift angles of 0.75%, 2.0% and 3.0% is shown in Figure 5. Until a drift of 1.5%, the damage process of the three wall specimens was almost the same. Cracks were observed at 0.25%, then yielding of the longitudinal reinforcement occurred at about 0.3% in all specimens. After that, W2R and W5 reached the maximum strength at 1.5%, and W4R at 3.0%. In W2R and W5, significant spalling of concrete occurred at 2.0% and reinforcement became exposed. In W4R, no spalling occurred at 2.0%, which was attributed to higher strength and lower stiffness of epoxy mortar compared to concrete, as shown in Table 5. In the second cycle of 3.0%, buckling of longitudinal reinforcement was observed in W2R and W5 and the load dropped to less than 60% of the maximum strength, at which point loading was terminated. On the other hand, in W4R, spalling of epoxy mortar was observed at 3.0%, but the reinforcement did not buckle. One of the longitudinal reinforcement bars fractured at 4.0% drift in the negative direction and buckling of other reinforcement occurred during the second cycle, so loading was terminated. It is thought that the reason why W4R retained the load up to 4.0% drift is that the concrete (or mortar) spalling area was smaller than that of W2R and W5, which provided additional buckling restraint to the longitudinal reinforcement.

The damage state of the beam specimens at 1.0%, 5.0% and the maximum drift angles is shown in Figure 6. Cracks were observed at 0.25%, and as drift increased, the number of cracks increased and the crack width expanded. G4R had no cracks form in the epoxy mortar, while wide cracks were observed directly above and below it (especially, at the boundary between the beam and the foundation). Yielding of the longitudinal reinforcement occurred at about 1.0% in all specimens. In G2R and G5, spalling of concrete and exposure of reinforcement occurred at 5.0%. After that, buckling of longitudinal reinforcement occurred at 6.0%, but no decrease of load was observed. On the other hand, G4R did not have spalling until the end of loading. Therefore, no exposure and buckling of reinforcement was observed. Finally, monotonic loading in the positive direction was applied after 6% drift. G2R and G5 did not fail until the stroke limit of the actuator (13%) was reached. In G4R, longitudinal reinforcement fractured at 11% and the load decreased rapidly, thus concluding the experiment. It is considered that the fracture of longitudinal reinforcement occurred because of strain concentration in the wide crack at the boundary between the beam and the foundation.

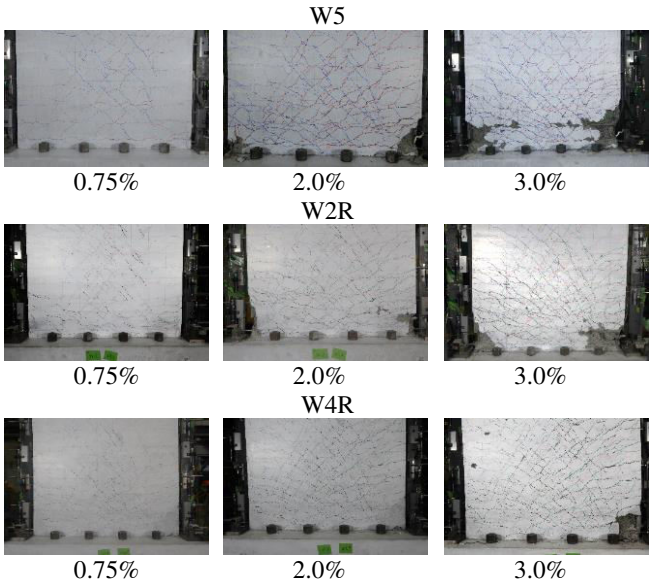

Figure 5: Damage process of wall specimens

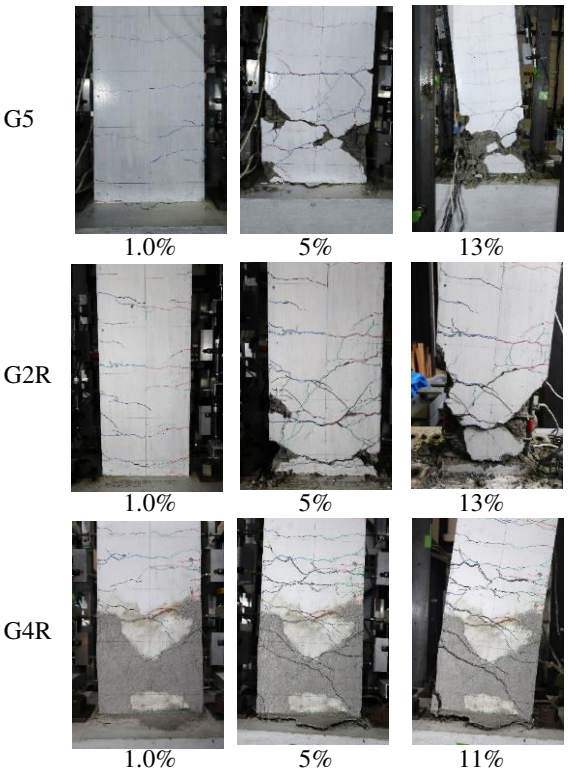

Figure 6: Damage process of beam specimens

3.2 Load – drift relationships

Shear force – drift relationships are shown in Figure 7 as comparisons between the original specimens (W5 or G5) and the repaired specimens (W2R, W4R, G2R or G4R). In the figures, yielding, maximum strength and longitudinal reinforcement buckling occurrences are shown as plots. In the negative direction of G4R, the yielding point is not shown because the strain gauge failed during the first loading before repair. The initial stiffness of W2R and G2R was lower than that of W5 and G5 (see Section 4 for details), but the hysteresis shapes after 0.5% were almost the same. Although W4R and G4R had lower initial stiffness than W5 and G5, the peak loads were higher than those of W5 and G5 after the 1% drift cycle. This is thought to be due to strain aging (Cottrell et al. 1949, Shegay et al. 2022) and strain hardening effects.

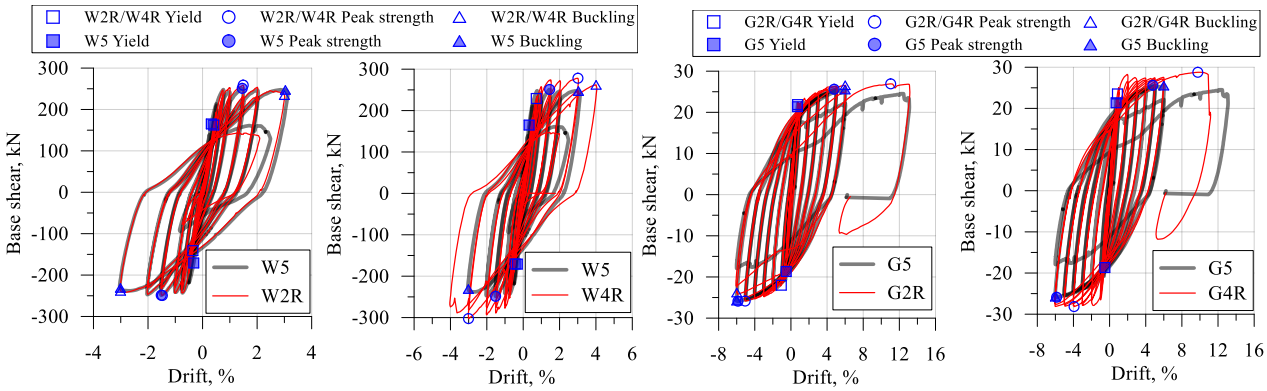

(a) Wall specimens (b) Beam specimens

Figure 7: Shear force – drift relationships

4 RECOVERY OF SEISMIC PERFORMANCE

4.1 Evaluation method of seismic performance recovery

Four factors to evaluate seismic performance recovery (initial stiffness φ_{si}, secant stiffness at the yielding point φ_{sy}, strength φ_q, and equivalent viscous damping φ_h) were calculated from the load - drift relationships of the original specimens and the repaired specimens. As shown in Figure 8, initial stiffness K_i and secant stiffness at the yielding point K_y were calculated as the secant stiffness to the first and second points on the tri-linear backbone approximation to the experimental load – drift backbones, respectively. The steps for developing the tri-linear backbone are shown in Figure 8 and are described below.

1. The point where load reached 1/3 of the maximum load was defined as a first backbone point.
2. Ultimate drift was assumed as 2.0% for the walls and 3.0% for the beams.
3. The stiffness of the third branch was assumed as zero. The second backbone point was decided by ensuring the energy absorption of the original backbone and the tri-linear backbone up to the ultimate drift are equal (i.e., A+C = B in Figure 8) and by minimizing the difference between the two backbones (i.e., minimize A+B+C).

Strength Q was defined as the load at the second backbone point (yielding point). Equivalent viscous damping h_{eq} was calculated by Equation (1).

$$h_{eq} = \frac{1}{4\pi} \cdot \frac{\Delta W}{(W_{pos}+W_{neg})/2} \tag{1}$$

where ΔW = hysteresis loop area of the second drift cycle; and W_{pos}, W_{neg} = strain energy in a positive and negative loading directions, respectively (shown in Figure 9).Seismic performance recovery factors (φ_{si}, φ_{sy}, φ_q and φ_h) were calculated as ratios of the performance of the repaired specimens (W2R, W4R, G2R or G4R) to that of the original specimens (W5 or G5), as shown in Equations (2) – (5). The backbones in the positive direction were used for calculation of φ_{si}, φ_{sy} and φ_q.

$$\varphi_{si} = K_i'/K_i \tag{2}$$

$$\varphi_{sy} = K_y'/K_y \tag{3}$$

$$\varphi_q = Q'/Q \tag{4}$$

$$\varphi_h = h_{eq}'/h_{eq} \tag{5}$$

where $K_i, K_y, Q \text{ and } h_{eq}$ = initial stiffness, secant stiffness at the yielding point, strength and equivalent viscous damping of an original specimen; and $K_i', K_y', Q' \text{ and } h_{eq}'$ = initial stiffness, secant stiffness at the yielding point, strength and equivalent viscous damping of a repaired specimen.

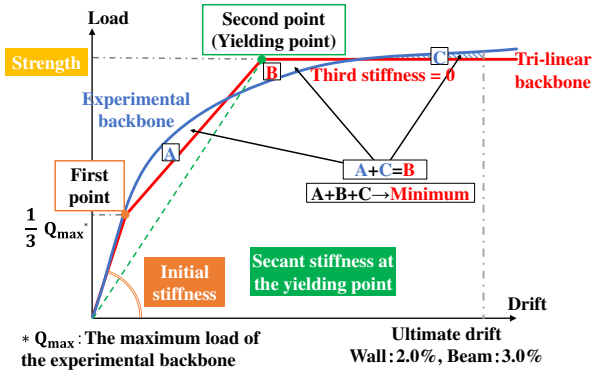

Figure 8: Tri-linear backbone approximation

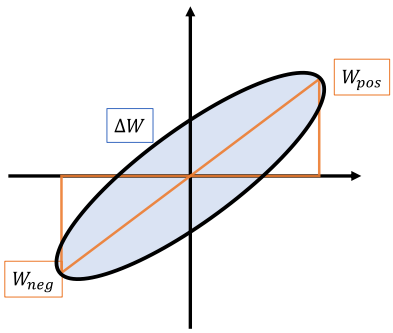

Figure 9: Equivalent viscous damping

4.2 Results of evaluation

The experimental backbone curves and the tri-linear backbone approximations for each specimen are shown in Figure 10 for lower drift levels. Recovery factors of initial stiffness, yielding stiffness and strength are shown in Figure 11. The initial stiffness recovery factors, φ_{si}, were in the range of 0.45-0.55 regardless of damage levels in both the walls and the beams. The yielding stiffness recovery factors, φ_{sy}, were 0.75 to 0.90 in the specimens of damage level IV (W4R, G4R), while they were 0.85 to 0.95 in the specimens of damage level II (W2R, G2R), which means smaller recovery of yielding stiffness in the severely damaged members. The strength recovery factors, φ_q, were about 1.0 in case of the damage II specimens and 1.1 to 1.2 in case of damage level IV. The reasons for the strength increase in the specimens of damage level IV are thought to be the high strength of epoxy mortar used for repair, strain aging (Cottrell et al. 1949, Shegay et al. 2022) and strain hardening of longitudinal reinforcement.

The recovery factors of equivalent viscous damping, φ_h, at each drift are shown in Figure 12. The recovery factors were 0.8-0.9 or more in W2R and G2R and 0.4-0.6 or more in W4R and G4R. The recovery factors increased as drift increased and reached about 1.0 at large drift levels in W2R and G2R. On the other hand, in W4R and G4R, the recovery factors were lower than those of W2R and G2R and did not reach 1.0. This is thought to be due to deterioration of bond between reinforcement and concrete by repetitive loading.

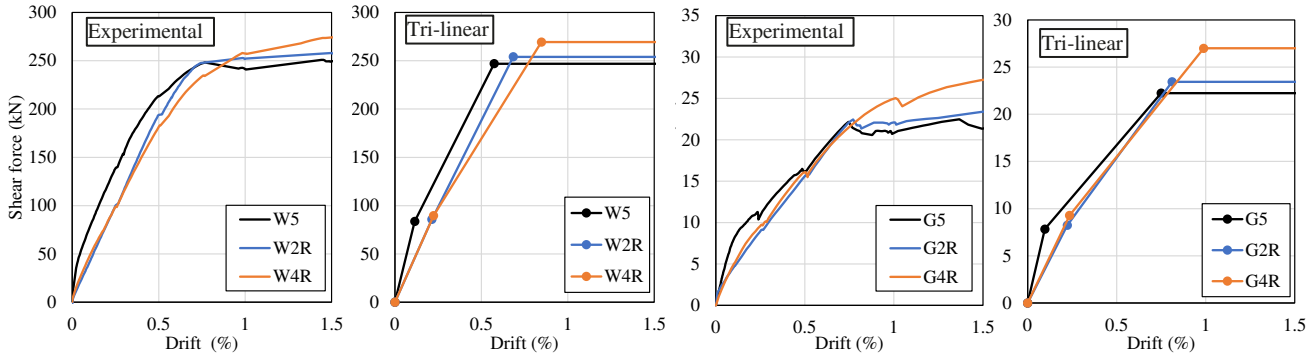

(a) Wall specimens (b) Beam specimens

Figure 10: Experimental backbone curves and tri-linear backbones at lower drift levels

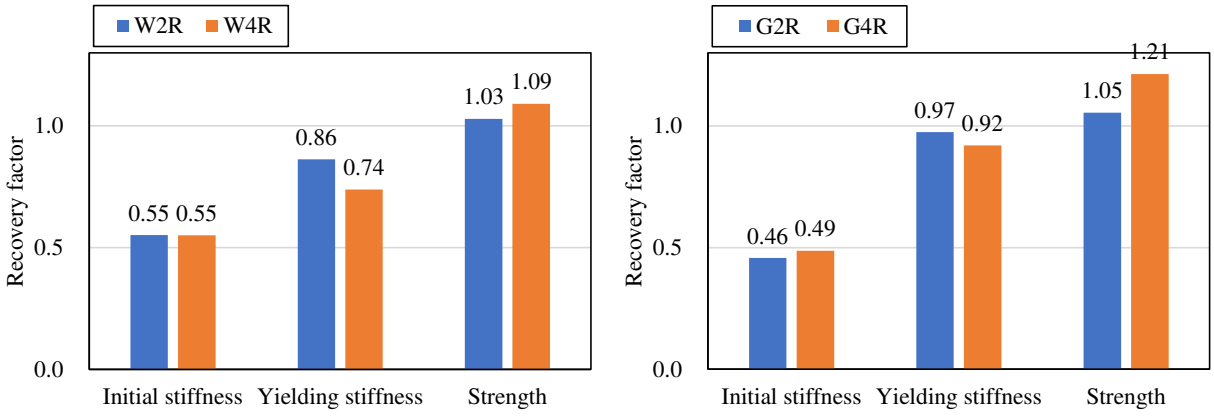

(a) Wall specimens (b) Beam specimens

Figure 11: Performance recovery factors of initial stiffness, yielding stiffness and strength

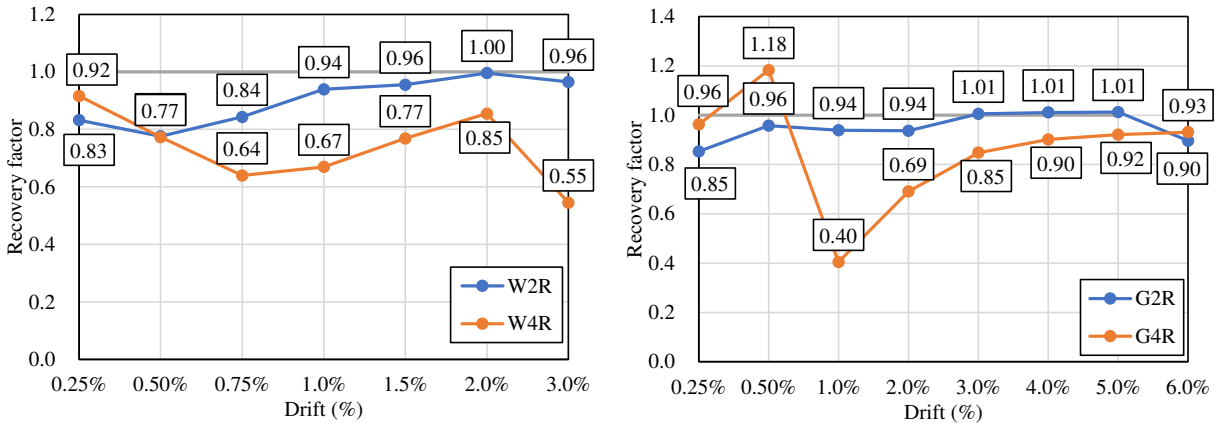

(a) Wall specimens

(b) Beam specimens

Figure 12: Performance recovery factors of equivalent viscous damping

5 CRACKING PROPERTIES

5.1 Classification of cracks

In the tests, cracks were visually observed both in the original specimens and the repaired specimens. In the repaired specimens, cracks were classified into three types, as shown in Figure 13 and described below.

1. New cracks: Cracks which newly occurred during loading of the repaired specimens.
2. Cracks which occurred in areas repaired by epoxy mortar.
3. Old cracks: Cracks which occurred during the first loading before repair and reopened during loading of the repaired specimens.

Crack width was defined as shown in Figure 13. The definition of 'reopening width' of old cracks shown in Figure 13(c) was calculated by Equation (6).

$$b_1 = b_2 - b_3 \tag{6}$$

where b_1= reopening width of old cracks; b_2= crack width observed during loading of the repaired specimens; and b_3= width of epoxy resin (equal to the crack width measured right before loading of the repaired specimens).

Crack patterns observed just before spalling of concrete (at 1.5% for the walls and at 4.0% for the beams) are shown in Figure 14. The orange lines indicate old cracks (including old cracks which did not reopen), the blue shade indicate repaired areas by epoxy mortar, and the green lines show the new cracks. Both bending and shear cracks were observed in the wall specimen, while predominantly bending cracks were observed in the beam specimen.

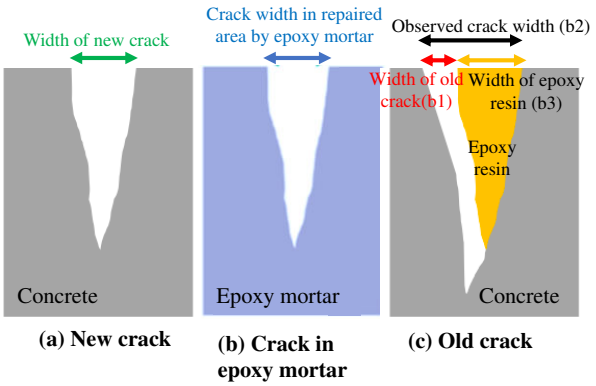

Figure 13: Classification of cracks

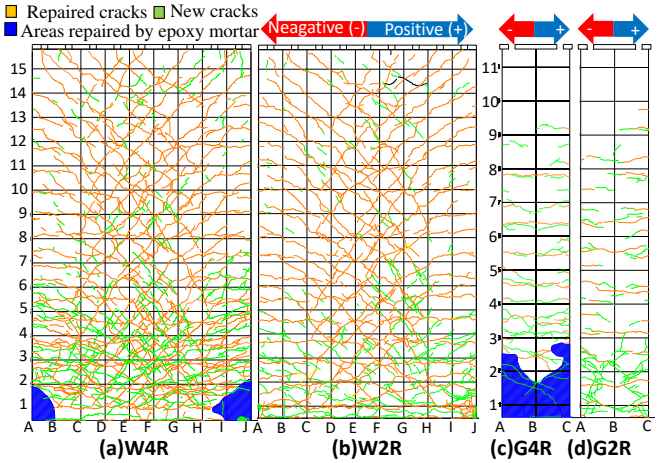

Figure 14: Observed cracks (just before concrete spalling)

5.2 Number of cracks

In the wall specimens, numbers and width of cracks were measured on the A and F lines (shown in Figure 14) for the positive direction loading, and on the E and J lines for the negative direction loading. In the beam specimens, they were measured on the A line for the positive direction loading, and on the C line for the negative direction loading. In the crack numbers and crack width results presented hereafter, the sum in the positive and the negative directions is reported.

The number of cracks at peak drift around yielding points (0.5% for the walls and 1.0% for the beams) and right before spalling of concrete (1.5% for the walls and 4.0% for the beams) are shown in Figure 15. At yielding points, the numbers of crack in the original specimens (W5 and G5) were similar to the number of old cracks in the repaired specimens (W2R, W4R, G2R and G4R). Since new cracks also occurred in the repaired specimens, the total numbers of cracks were larger than those of the original specimens. On the other hand, at drift just before concrete spalling, only a small number of additional old cracks reopened in the repaired specimens, while new cracks increased.

The reopening ratios of repaired cracks, r_{op}, are shown in Figure 16. The reopening ratios r_{op} were calculated by Equation (7).

$$r_{op} = n_{op}/n_r \tag{7}$$

where n_{op}= number of old cracks; and n_r= number of repaired cracks

At yielding points (0.5% for the walls and 1.0% for the beams), the reopening ratios, r_{op}, were between 60% and 80% in the walls and between 40% and 60% in the beams. This shows that around half or more of the repaired cracks reopened at small drift ratios and was thus the likely cause of deterioration of initial stiffness shown in Section 4.2. The reopening ratios increased with increasing drift; however, a peak is reached at some point lower than 100%. The r_{op} values were higher in the walls and in the specimens of damage level II. The reasons will be investigated in the next section by considering crack width.

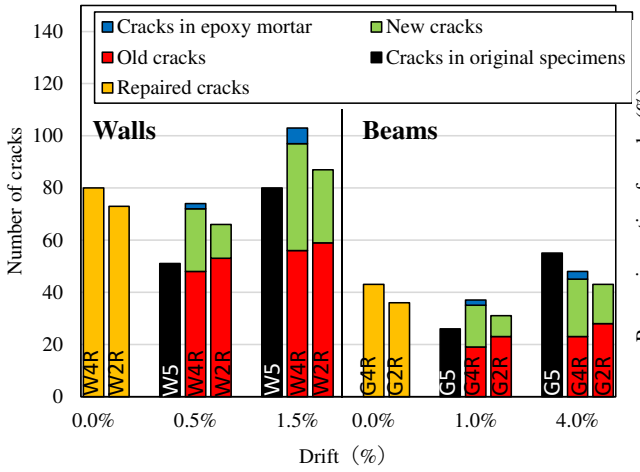

Figure 15: Number of cracks

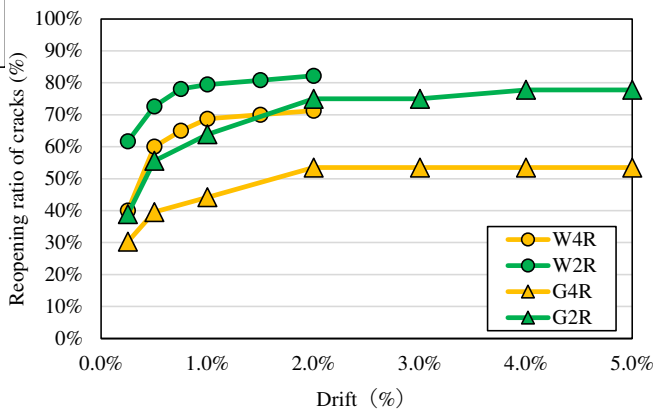

Figure 16: Reopening ratios of cracks

5.3 Crack width

The sum of measured crack width at peak drift around yielding points (0.5% for the walls and 1.0% for the beams) and right before spalling of concrete occurred (1.5% for the walls and 4.0% for the beams) is shown in Figure 17. At both points, the crack width sums are almost the same between the original specimens and the repaired specimens.

The ratio of the sum of old crack width to the total crack width, r_{oc}, is shown in Figure 18. This ratio was calculated by Equation (8).

$$r_{oc} = \Sigma w_o/(\Sigma w_o + \Sigma w_n + \Sigma w_m) \quad (8)$$

where Σw_o= sum of old crack width; Σw_n= sum of new crack width; and Σw_m= sum of crack width in the epoxy mortar.

At small drift, the r_{oc} is the highest. This result can explain why the deterioration of initial stiffness occurred.

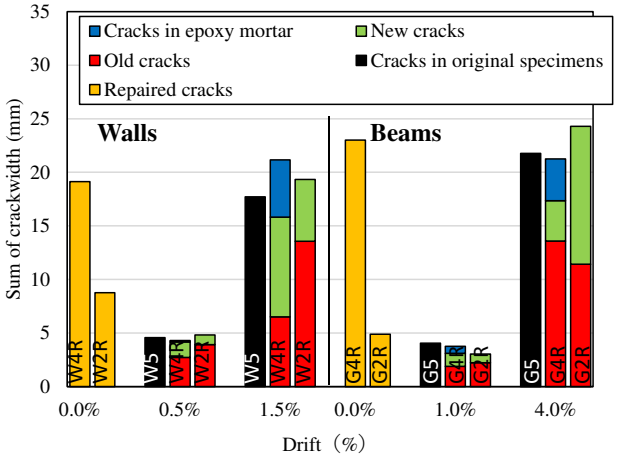

Figure 17: Sum of crack width

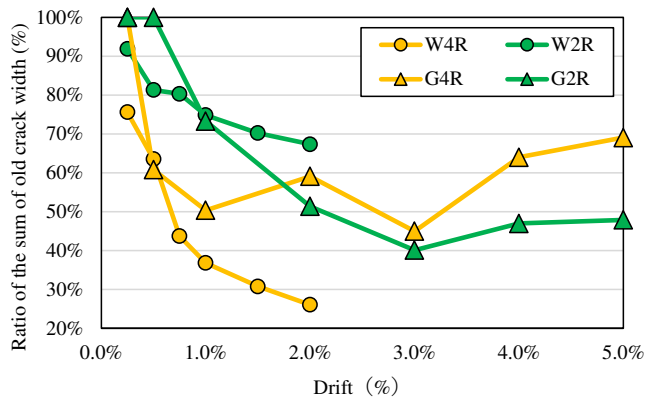

Figure 18: Ratios of the sum of old crack width to the total crack width

The relationship between the maximum crack width observed before repair (at the maximum drift of W2, W4, G2 and G4) and old crack width (reopening width of repaired crack at the same drift) in the repaired specimens is shown in Figure 19(a). In other words, the data in this figure is a comparison of crack width of given cracks before and after repair. The data in Figure 19(a) suggests that the larger the crack width is

before repair, the smaller this crack width will become after repair. A plot showing the crack width after repair normalized by its width before repair is shown as Figure 19(b). The data in this plot shows suggests that cracks that were larger than 0.2 mm before repair are not likely to reopen after repair. Based on this, it is considered that epoxy injection was most effective on wide cracks (>0.2 mm). For further investigation on the relationships between epoxy penetration and crack width in each specimen, average crack width before repair w_{av} was calculated as:

$$w_{av} = \Sigma w / n_r \tag{9}$$

where Σw= sum of crack width before repair (at the maximum drift before repair); and n_r= number of repaired cracks.

The average crack width w_{av} is 0.12 mm in W2R, 0.23 mm in W4R, 0.14 mm in G2R and 0.54 mm in G4R. It is clear that the w_{av} values are lower in the specimens with damage level II, and lower in the walls than in the beams. Therefore, the higher reopening ratios of repaired cracks in the specimens with lower damage levels and the walls shown in Figure 16 can be attributed to difficulty in epoxy injection due to small crack width.

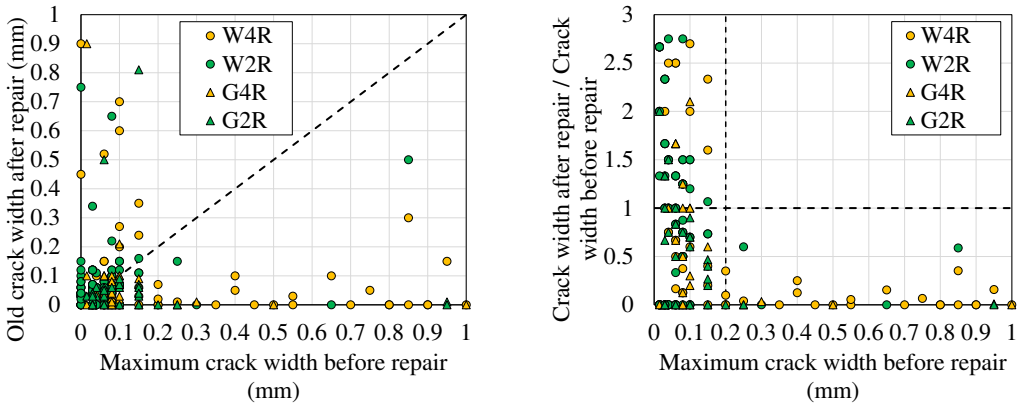

(a) Crack width before repair and after repair (b) Ratios of crack width before repair to that after repair

Figure 19: Relationship between the maximum crack width before repair and old crack width after repair

6 CONCLUSIONS

Three RC beam and three RC wall specimens with different damage levels (moderate and severe) were subjected to pseudo-static loading to determine the seismic performance recovery following repair. Based on the test results, the following conclusions can be drawn.

1. Spalling of concrete in the repaired specimens (severely damaged) was less than that observed in the original specimens due to high strength and low stiffness of epoxy mortar used in repair.
2. Initial stiffness recovery of 0.45 to 0.55 of the original members was achieved, regardless of the initial damage level. Secant stiffness at the yielding point of the repaired members recovered 0.85 to 0.95 in moderately damaged specimens while in severely damaged specimens, recovery was 0.75 to 0.90. Structural strength of the repaired members was found to be equivalent to that of the original members in moderately damaged cases and 1.1 to 1.2 in severely damaged cases. Energy absorption capacity recovery was more than 0.8 in moderately damaged members and more than 0.4 in severely damaged members.
3. Crack characteristics were studied based on visual observations taken during the experiment. It was observed that more than half of the cracks injected with epoxy resin reopened upon loading, which

explained the low recovery of initial stiffness. Crack width data showed that wider cracks are generally less likely to reopen following repair because of better epoxy penetration.

7 ACKNOWLEDGEMENT

The research presented in this paper was carried out under joint research between Tohoku University and Obayashi Corporation and funded by the Consortium for Socio- functional Continuity Technology (http://www.softech.titech.ac.jp/; Project ID: JPMJOP1723 under Japan Science and Technology Agency). The authors would like to express their gratitude for the support.

8 REFERENCES

Applied Technology Council (ATC-43 Project). 1995, *Evaluation of Earthquake Damaged Concrete and Masonry Wall Buildings (FEMA 306).* Redwood City: Applied Technology Council.

Japan Building Disaster Prevention Association (JBDPA). 2015, Guidelines for Post-earthquake Damage Evaluation and Rehabilitation of RC Buildings. *Tokyo*: Japan Building Disaster Prevention Association.

Shegay, A., Miura, K., Mikawa, A., Maeda, M. & Seki, M. 2023. Performance recovery of a repaired 4-storey reinforced concrete structure subjected to shake-table testing, *Earthquake Engineering & Structural Dynamics,*1-21.

Cottrell, AH. & Bilby, BA. 1949. Dislocation theory of yielding and strain ageing of iron, *Proceedings of the Physical Society*, Vol 62(1), 49-62

Shegay, A., Mikawa, A., Miura, K. & Maeda, M. 2022. Characteristics of strain ageing in SD345 reinforcement and its effects on repaired structures, *Proceedings of Annual Meeting of Japan Association for Earthquake Engineering,*